

## Article

# Influence of Piston Lubricant on the Distribution of Defects in Cold Chamber High Pressure Die Casting

Jingzhou Lu <sup>1</sup>, Ewan Lordan <sup>2</sup>, Yijie Zhang <sup>2</sup>, Zhongyun Fan <sup>2</sup> and Kun Dou <sup>1,\*</sup>

<sup>1</sup> School of Metallurgy and Environment, Central South University, Changsha 410083, China; 213506005@csu.edu.cn

<sup>2</sup> Brunel Centre for Advanced Solidification Technology (BCAST), Brunel University London, London UB8 3PH, UK; ewan.lordan@brunel.ac.uk (E.L.); robertzyj@163.com (Y.Z.); zhongyun.fan@brunel.ac.uk (Z.F.)

\* Correspondence: kun.dou@csu.edu.cn; Tel.: +86-17600802394

**Abstract:** In the cold chamber high pressure die casting process (CC-HPDC) for light alloys, the piston lubricants play a key role in protecting the piston tip from wearing and ensure adequate seal with the shot sleeve. However, during the production process, the pouring of overheated aluminum alloy melt into the shot sleeve would lead to evaporation and burning of the lubricants once in contact with the piston tip. The burning products, however, would form gas and non-metallic inclusions in the melt which would be transported and injected into the die area and finally trapped in the castings, all of which would affect the mechanical properties of the as-cast samples and deteriorate the product quality. To further investigate this issue, a pilot scale HPDC machine is used and the lubricant burning issue is studied based on material characterization and numerical modelling. The chemical composition, size, and morphology of the burned products are observed using scanning electron microscope (SEM) and energy dispersive spectrometer (EDS). In order to better explore the issue of lubricant combustion discovered in the experiment, a finite element model describing the entire HPDC process is established and the burning, motion, and trapping of the lubricant are calculated. The final distribution of the burned products such as gas and non-metallic inclusions are predicted and their influence on final solidification quality of the as-cast products under various process parameters are analyzed qualitatively. Finally, a slow shot velocity range of 0.4–0.6 m/s and an acceleration profile that ramps up to 0.3 m/s over 0–370 mm of the shot sleeve proved to be the most effective in reducing air entrainment and oxide inclusions to alleviate the burning of lubricant on final product quality.

**Keywords:** high pressure die casting; lubricant; solidification; mathematical modelling; defects formation



Received: 23 January 2025  
Revised: 15 February 2025  
Accepted: 22 February 2025  
Published: 24 February 2025

**Citation:** Lu, J.; Lordan, E.; Zhang, Y.; Fan, Z.; Dou, K. Influence of Piston Lubricant on the Distribution of Defects in Cold Chamber High Pressure Die Casting. *Lubricants* **2025**, *13*, 99. <https://doi.org/10.3390/lubricants13030099>

**Copyright:** © 2025 by the authors. Licensee MDPI, Basel, Switzerland. This article is an open access article distributed under the terms and conditions of the Creative Commons Attribution (CC BY) license (<https://creativecommons.org/licenses/by/4.0/>).

## 1. Introduction

In the CC-HPDC process, commonly used for producing light alloy components, piston lubricants play a crucial role in reducing wear and ensuring proper sealing between the piston and shot sleeve. However, at high temperatures, particularly when molten metal is poured into the shot sleeve, these lubricants can evaporate and combust upon contact with the piston tip. The resulting combustion products—comprising gases and non-metallic inclusions—become entrained in the melt, which is subsequently injected into the die cavity. These contaminants can lead to various casting defects, such as gas porosity and oxide inclusions, ultimately degrading the mechanical properties and overall quality of the final product [1–6]. Understanding how lubricant combustion influences melt flow and

defect formation is therefore essential for optimizing the CC-HPDC process and improving casting quality [7–9].

Previous research has extensively investigated defect formation and process optimization in HPDC. Tsoukalas [10] demonstrated that optimizing piston velocity, intensification pressure, and filling time can significantly reduce porosity. Jiao et al. [11] studied the influence of slow-shot speed on primary silicon particle (PSP) distribution and porosity in AlSi17Cu2.5 alloy, highlighting the role of controlled injection profiles in improving casting integrity. Fiorese et al. [12] further linked plunger kinematics to defect formation, emphasizing the importance of motion control.

Numerical simulations have also been widely applied to study melt flow and defect formation. Cleary [13] validated flow models through interrupted filling tests, while Gerald [14] optimized the ingate liquid jet using the smoothed particle hydrodynamics (SPH) method. Cica et al. [15] developed a predictive porosity model using fuzzy systems and genetic algorithms. Additionally, studies by Li et al. [16], Xu et al. [17], and Niu et al. [18] explored defect formation under different process conditions through numerical and experimental approaches.

While these studies provide valuable insights, they primarily focus on machine parameters, melt flow, and thermal effects, while overlooking the role of lubricant combustion in defect generation. The specific contribution of combustion products to air entrainment, non-metallic inclusion formation, and overall casting quality has not been systematically studied. Furthermore, an integrated approach combining experimental characterization and numerical modeling to assess lubricant combustion effects remains lacking.

This study uniquely combines material characterization (SEM: TESCAN MIRA 3 LMU, EDS: Oxford X-Max20) and finite element modeling (FEM) to investigate the previously overlooked impact of lubricant combustion on defect distribution in CC-HPDC. By analyzing the composition, size, and morphology of combustion products and simulating the HPDC process, this research provides new insights into the role of lubricant combustion in air entrainment, non-metallic inclusion formation, and melt flow. The findings offer a novel perspective on defect formation mechanisms, contributing to process optimization and product quality improvement while addressing critical gaps in existing research.

## 2. Phenomenon Discovery and Experimental Methods

### 2.1. Phenomenon Discovery

During HPDC experiments, we initially observed the presence of oxides, gas pockets, and inclusions in the cast samples. This issue arises because, during production, pouring overheated molten metal into the shot sleeve causes the lubricants to evaporate and combust upon contact with the piston tip. The combustion by-products generate gases and non-metallic inclusions within the melt, which are subsequently transported into the die cavity and trapped in the castings. These inclusions adversely affect the mechanical properties of the as-cast samples and significantly degrade product quality.

Figure 1a presents a typical micrograph of an inclusion located on the fractured surface of the tensile specimen (in cross-sectional direction), where large non-metallic inclusions are visible within the pores. Oxides are also detected near these inclusions. Pores typically form at non-wetted interfaces, with potential nucleation sites including non-wetted surfaces of oxide films and specific non-metallic inclusions—especially those containing low-surface-tension liquids or non-wetted solids. It is likely that these inclusions, along with associated oxides, serve as nucleation sites for the pores observed in the specimens. Previous research on the EDX analysis of fracture surfaces revealed that these inclusions typically contain elements such as C, Na, S, Cl, K, and Ca [19]. However, the presence of C alone, due to its low atomic mass, is insufficient to confirm the pyrolysis hypothesis, as C is a common

contaminant in electron microscopy. Therefore, we focus on the heavier elements, namely Na, S, Cl, K, and Ca. Petrochemical or synthetic additives are often incorporated into lubricant base stocks to enhance their performance. Under severe mechanical or thermal loading, the lubricating film may rupture, causing direct asperity-asperity to contact on the metal surface. Extreme pressure (EP) additives, as their name suggests, improve lubrication under high-pressure conditions. These additives often contain compounds of S or Cl, which become reactive at elevated temperatures, releasing derivatives of S or Cl. These derivatives react with exposed metal surfaces to form protective compounds (e.g., FeS or FeCl<sub>3</sub>), creating a thin solid layer that mitigates wear. Additionally, other additives such as surfactants and thickeners are common in commercial lubricants, often containing Na, K, and Ca compounds. To test the pyrolysis hypothesis, filling tests were conducted by allowing the liquid to solidify in the shot chamber while the piston remained stationary. Figure 1b shows a photograph of one of these filling test samples, with a close-up provided in Figure 1c. In Figure 1b, the location of the pouring hole is labeled as the “inlet”, and during the experiment, the plunger was in contact with the left-hand surface of the billet. As shown in Figure 1c, large films are present on the billet surface, resembling the non-metallic inclusions observed in Figure 1a. These findings suggest that the non-metallic inclusions may originate from the pyrolysis of commercial plunger lubricants. Although it could be argued that the detected elements might come from foundry fluxes, no flux was employed in these experiments.

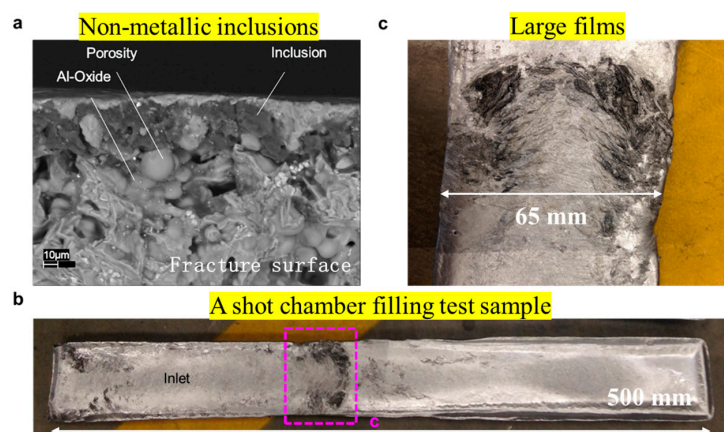


**Figure 1.** Source of non-metallic inclusions. (a) Micrograph showing a representative non-metallic inclusion observed on the fracture surface of a fatigue specimen extracted from an automotive component. (b) Image of a shot chamber filling test sample, with the inlet corresponding to the pouring hole. (c) Enlarged view of the dashed region highlighted in (b).

## 2.2. HPDC Experiment

A pilot-scale high-pressure die casting (HPDC) machine was employed to address the issues of lubricant combustion and non-metallic inclusions identified in HPDC casting experiments. The combustion phenomena were analyzed through material characterization and numerical simulation. The chemical composition, size, and morphology of combustion products in the castings were investigated using scanning electron microscopy (SEM) and energy dispersive spectroscopy (EDS). The alloy used in this study was Silafont-36 (Al-9Si-0.3Mg-0.5Mn). A 40 kg crucible of Silafont-36 was melted in an electric resistance furnace and held at 750 °C for 30 min to ensure a uniform composition. The Silafont-36 alloy was selected due to project requirement and the optimal parameters for pouring temperature and homogenization time were determined based on multiple sets of experiment trials. The melt was then degassed using a high shear melt conditioning (HSMC) device [20], which consisted of two stages: (i) degassing for 10 min at a rotor speed of 1500 rpm and an argon

flow rate of 0.2 L/min, followed by (ii) intensive melt shearing for 20 min without argon flow. Following melt treatment, the molten metal was transferred into the shot sleeve of a FRECH 4500 kN locking force cold chamber HPDC machine using a transfer ladle. The process parameters were controlled with the melt temperature maintained at 680 °C, the shot sleeve at 180 °C, and the die cavity at 150 °C. The molten metal was injected into the die cavity at a slow shot speed of 0.3 m/s and a filling speed of 3.6 m/s to produce eight round tensile samples. These samples, with a nominal gauge diameter of 6.35 mm, were manufactured in accordance with ASTM (American Society of Testing Materials) E8/E8M standards [21]. During experiments, different slow shot and filling speeds were selected to evaluate their influence on the casting process. The geometry of the tensile samples and gating system has been previously detailed in earlier studies [20].

### 2.3. Numerical Simulation Methods

A finite element model (FEM) was developed to simulate the entire HPDC process, accounting for lubricant combustion, movement, and entrapment. Using the ProCAST software platform (ProCAST 13.5), FEM mesh generation, model discretization, and result analysis were performed systematically. The final distribution of combustion products, such as gases and non-metallic inclusions, was predicted, and their effects on the solidification quality of as-cast products were qualitatively analyzed under various process parameters. The geometrical model of the HPDC system was created using 3D modeling software (Figure 2a). To enhance computational efficiency, only half of the model was used for simulations.

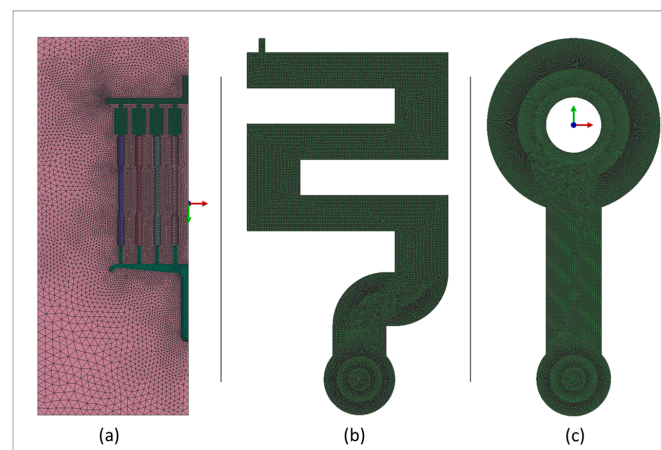


**Figure 2.** FEM models (a) HPDC system model. (b) Round-mold model. (c) S-shape model.

Initially, the die temperature was set to room temperature (25 °C). As the HPDC process began, heating channels located in the mobile and stationary dies were activated to raise the die temperature to the target working temperature of 180 °C. Once the target temperature was reached, the heating channels were switched off. In the simulation, a dynamic heat boundary condition was applied to the dies based on the timing and sequence data, allowing the calculation of the die's temperature distribution. Air entrainment during HPDC, caused by turbulent flow and fluid atomization, was incorporated into the model using the GAS model [22]. The transport and accumulation of oxides were modeled using an oxide indicator, measured in units of  $\text{cm}^2 \cdot \text{s}$ , which represents the free surface area multiplied by time. The calculated indicator values were transported with the fluid flow and free surface. The impact of intensification pressure on the solidification process was managed in the model through a critical gate solid fraction. Liquid feeding was assumed to cease when the solid fraction in the gate exceeded a critical threshold of 0.9, effectively controlling the solidification dynamics. In addition, round-mold and S-shape

model were established in the same way for numerical simulation work and compared with experimental results in existing literature to verify the accuracy of the air entrainment model (Figure 2b,c). The specific model and results will be described in detail in Chapter 3.

### 3. Experimental Results and Model Validation

#### 3.1. Electron Microscopy Observation of Casting Samples

During the casting process, the metal is heated to over 600 °C for a short period of time, during which the lubricant burns. Mixed with the liquid aluminum, the inclusions and gases are transported by the plunger through the gate into the casting, and after being pressed at high temperature, the gas eventually forms pinholes and porosity. At the same time, oxides are also carried into the casting.

The tensile specimens obtained from earlier HPDC casting trials were extracted and tested for as-cast mechanical properties. After that, the tensile fracture surfaces were observed using SEM fractography. Key casting defects, such as oxide films, porosity, and non-metallic inclusions were detected, with a representative backscatter electron (BSE) micrograph provided in Figure 1a. In all tensile samples with varying strengths, inclusions were detected (Figure 3). Large non-metallic inclusions are observed within the pore. An enlargement of one of the tensile samples (Ultimate Tensile Strength, hereinafter as UTS: 278.4 MPa, Elongation, hereinafter as EL: 7.12%) revealed distinct oxide inclusions and shrinkage porosity. In the first tensile sample (Figure 4) (UTS: 275.4 MPa, EL: 6.38%), the elemental distribution at the surface of the thin oxide film was analyzed, with a more detailed examination focused on the region within the red box. Elemental analysis showed the presence of C, Al, O, Si, which indicates the formation of non-metallic inclusions.

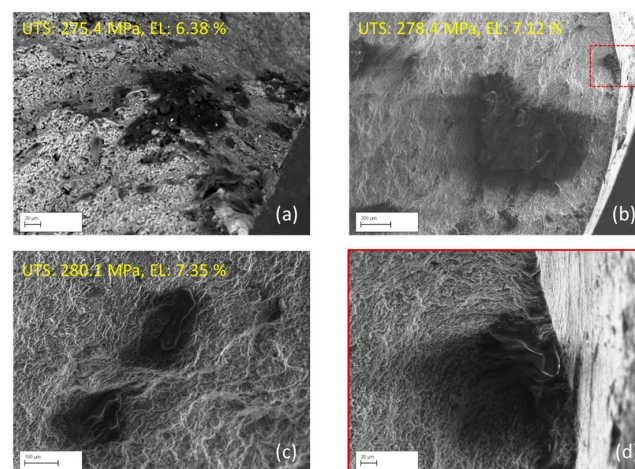


**Figure 3.** Observation of fracture surfaces of samples with different tensile strengths obtained by HPDC. (a) UTS: 275.4 MPa, EL: 6.38%; (b) UTS: 278.4 MPa, EL: 7.12%; (c) UTS: 280.1 MPa, EL: 7.35% (d) Enlarged red area in (b).

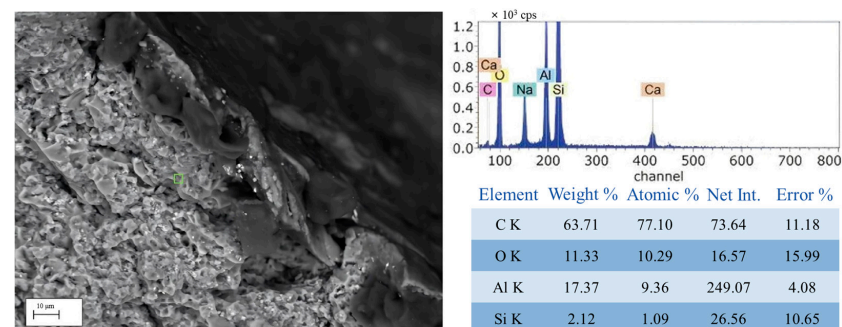


**Figure 4.** EDS results of tensile sample fracture surface.

### 3.2. Verification of Numerical Simulation Methods

To validate the accuracy of the simulated fluid flow patterns generated by the established model, two classical HPDC experimental results from Cao et al. and Homayonifar et al. [23] were used as benchmarks. The comparisons between the experimental data and the simulation results generated using models from this work are presented in Figure 5. These comparisons demonstrate that the mathematical model developed in this study accurately predicts the fluid flow behavior and air entrainment during the die-filling stage of the HPDC process.

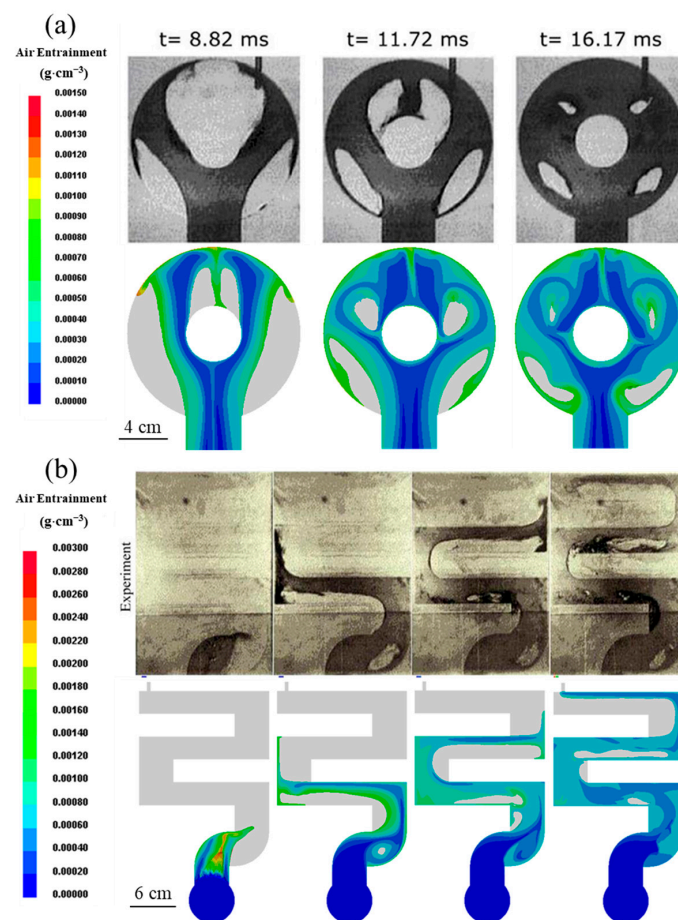


**Figure 5.** Flow field validation between experiments and modelling during the filling process for the (a) Round-mold model and the (b) S-shape model.

To further validate the model's suitability in prediction of defects such as inclusions, trapped air, and porosities, relative modelling and corresponding casting trials are conducted to compare the formation and distribution of porosities, air entrainment and inclusions in the casting system, which is illustrated in Figure 6. In the modelling results, the purple area indicates the distribution of gas and shrinkage porosities, and the blue area indicates the existence of inclusions in the castings. In the real casting trials, as-cast castings are extracted from the HPDC machine and various locations are cut, polished, etched, and observed using SEM before being compared with modelling results. It could be clearly seen that in the casting system, the overflow part contains mainly large porosities, and the bottom part contains mainly trapped gas-induced porosities. In the center region, there is a limited number of gas and porosities, and while several inclusions exist, the observation and modelling results are in good correspondence.

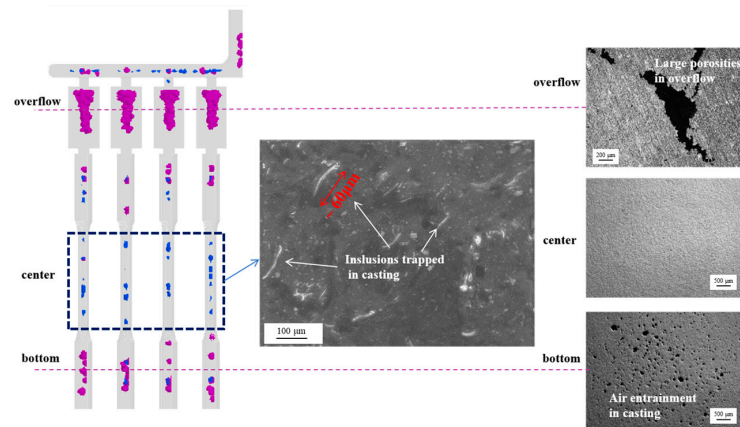


**Figure 6.** Prediction and observation of defects in corresponding parts in the casting system.

## 4. Prediction of the Final Distribution of Combustion Products

### 4.1. The Motion Behavior of Oxides Generated by Lubricant Combustion During HPDC Process

In Figure 7, the oxides continuously rise to the surface during the slow shot phase. Additionally, due to the absence of a protective atmosphere as the piston advances, some of the melt surface is oxidized by air. These oxides accumulate on the melt surface, gradually forming a layer of oxide film. As the piston moves forward, the oxides accumulate at the front. During the melt injection phase, some of the oxides flow into the tensile sample area with the fluid, while most remain in the shot sleeve. Ultimately, the change in oxide concentration per unit area per unit time (i.e., diffusion rate) in the tensile sample region is approximately  $6.0 \text{ cm}^2 \cdot \text{s}$ .

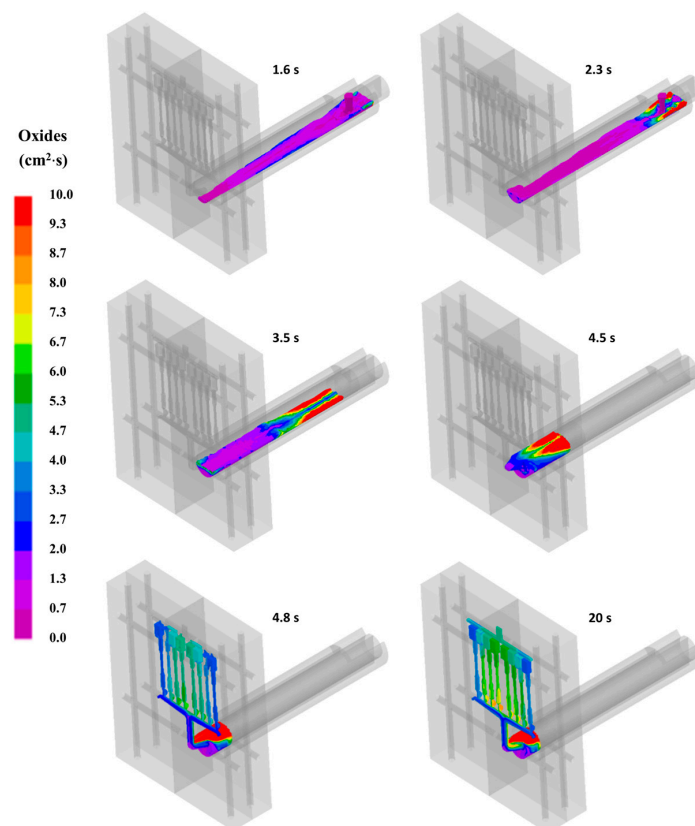


**Figure 7.** Distribution of oxides during die-casting process.

#### 4.2. Influence of Slow Shot Velocity on Defects Formation

Using the validated mathematical model, the pre-filling behavior and free surface evolution of the melt in the shot sleeve were simulated. Slow shot velocities were set to 0.2–0.3 m/s, 0.4–0.6 m/s, and 0.6–1.0 m/s. Figures 8–10 depict the formation of the shot wave and the air entrapment occurring during the shot sleeve filling process.

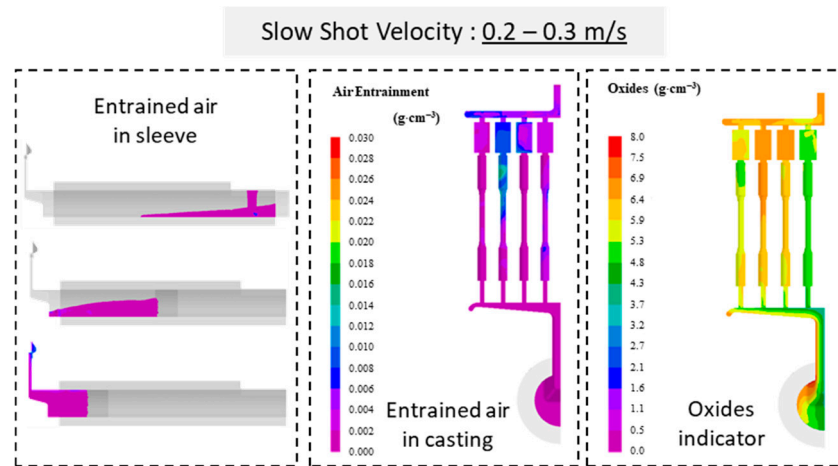


**Figure 8.** Air entrapment in casting samples at a slow shot velocity of 0.2–0.3 m/s.

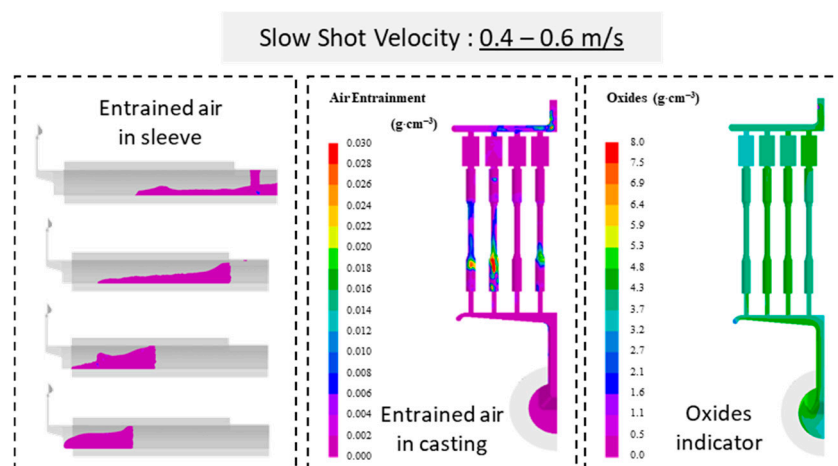


**Figure 9.** Air entrapment in casting samples at a slow shot velocity of 0.4–0.6 m/s.

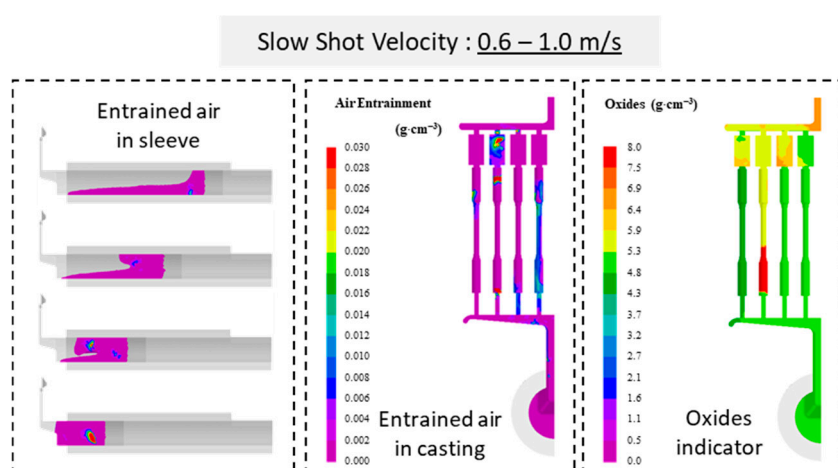


**Figure 10.** Air entrapment in casting samples at a slow shot velocity of 0.6–1.0 m/s.

It is clear from the simulation results that during the slow shot phase (0.2–0.3 m/s) under baseline conditions, the melt flow is initiated by the movement of the piston, and the free surface remains relatively calm, with minimal air entrainment during both filling and injection (Figure 8). In the casting region, air entrainment is not severe, with an overall low entrainment level primarily concentrated near the runner and gate areas. Only a slight amount of gas entrainment, approximately  $0.01 \text{ g/cm}^3$ , is observed in the upper portion of one tensile sample. However, oxides are carried from the filling area into the casting region, with oxide inclusions mainly concentrated near the runner and mold cavity entrance, showing relatively high values. Some tensile samples exhibit severe oxide inclusions, approximately  $4.8\text{--}6.9 \text{ cm}^2\cdot\text{s}$ . Under low-speed conditions, the metal flow remains relatively stable, but the extended exposure time of the liquid metal surface increases the likelihood of oxide formation.

When the piston slow shot velocity is increased to 0.4–0.6 m/s, a wave forms at the free surface front, though air entrainment remains minimal (Figure 9). The air entrainment in the casting region is slightly more severe compared to the 0.2–0.3 m/s condition, but it remains relatively acceptable, with entrainment observed only in certain areas of the tensile samples. The increased velocity accelerates the flow of the molten metal, leading to greater air entrapment, though the higher speed may also cause localized breaking of entrained air pockets. In contrast, the oxide inclusion condition is improved, with a relatively stable distribution across the casting region, averaging around  $4.3 \text{ cm}^2\cdot\text{s}$ . The medium-speed flow reduces surface exposure time and minimizes the breakage and entrainment of oxide films, though some localized inclusions are still present.

Further analysis of the melt flow was conducted by increasing the piston velocity to 0.6–1.0 m/s (Figure 10). In this case, as the piston accelerates, the melt's free surface accumulates and contacts the top of the chamber before collapsing. During this phase, a portion of the air is captured at the fluid front, which is subsequently transported into the die cavity and remains in the final casting. The air entrainment within the casting is more evenly distributed but has a noticeably higher density compared to the two lower-speed conditions. This is because the higher flow velocity increases air entrainment, and the faster speed disperses the entrained air throughout the casting. Oxide inclusions also increase significantly, particularly within the runner and casting regions, with red zones indicating areas of high oxide concentration. The high-speed jet intensifies turbulence in the metal flow, making surface oxides more likely to be drawn into the molten metal, leading to a greater amount of oxide inclusions.

From these comparisons, it can be concluded that to minimize air entrainment, the piston velocity during the slow shot phase should not exceed 0.6 m/s. Additionally, lower slow shot velocities result in more severe oxide inclusions.

#### *4.3. Motion and Distribution of Particles of Different Sizes*

The particle trajectory distribution map was plotted (Figure 11), and it can be observed that finer particles travel further along the flow field, resulting in a broader distribution. In contrast, larger particles only travel shorter distances, leading to a more localized distribution. The larger particles (100 microns) show relatively smooth and stable trajectories in the tensile sample region. This stability minimizes the potential for turbulence-induced defects and ensures uniform filling of the tensile sample. However, due to their larger size and higher inertia, these particles may not adapt well to sudden changes in flow direction, potentially leading to poor flow in complex geometries or insufficient filling in intricate areas. The smaller particle size (20 microns) allows for greater adaptability to the flow dynamics, potentially enabling better filling of complex geometries within the tensile sample. However, increased dispersion and irregular trajectories may introduce turbulence,

leading to flow instabilities and potential defects such as air entrapment or non-uniform microstructure. Highly responsive to flow, 15-micron particles are enabled to reach finer details in the tensile sample region. This property is advantageous for ensuring complete filling of intricate areas. However, highly chaotic and dispersed trajectories make the flow pattern unpredictable, increasing the likelihood of turbulence and associated defects, such as porosity or oxide entrapment, which could compromise the mechanical properties of the tensile sample.

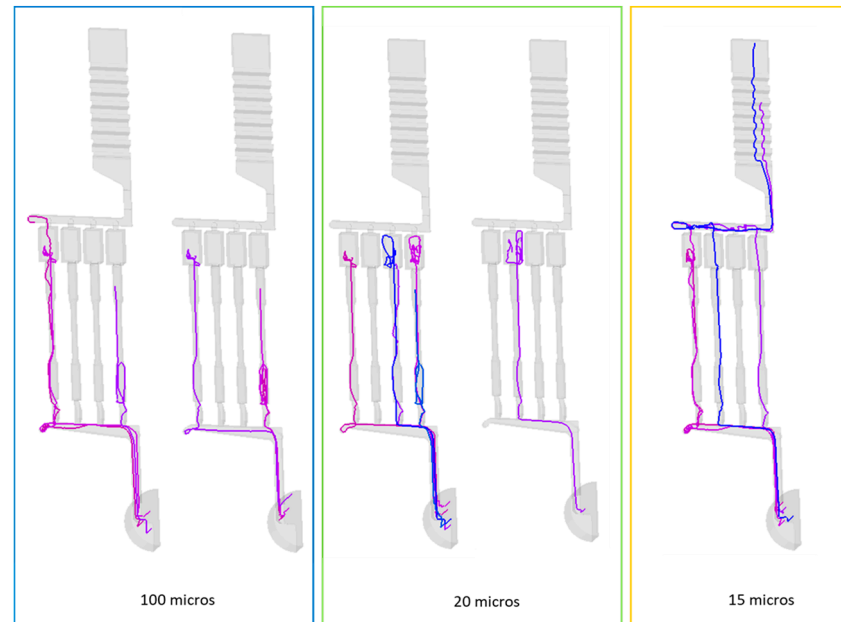


**Figure 11.** The motion trajectory of particles of different sizes in the mold.

#### 4.4. Influence of Piston Slow Shot Acceleration on Defects Formation

HPDC simulation experiments were conducted using six different slow shot acceleration profiles, which are as follows: acceleration from 0 to 0.2 m/s within 10 mm, 30 mm, 50 mm, and 60 mm, acceleration from 0 to 0.3 m/s within 50 mm, and acceleration from 0 to 0.3 m/s within 370 mm (Figure 12). The relationship between position and velocity for each slow-shot acceleration profile was plotted (Figure 13). The segment from 0 to 370 mm represents the slow-shot phase, while the range from 405 to 450 mm corresponds to the rapid injection phase. The results of gas entrapment were subsequently obtained.

From Figure 14, it can be observed that conditions 1, 2, and 5 exhibit relatively severe air entrapment, with some areas reaching the red level (i.e., air entrapment greater than  $0.002 \text{ g/cm}^3$ ). Additionally, for conditions 2 and 5, the tensile samples in certain regions show significant air entrapment, which could severely affect the tensile properties of the castings. Conditions 3 and 4 have similar levels of air entrapment, with some entrapment present, but the distribution is relatively uniform, and the levels are not as high. The optimal condition is found to be condition 6, where the air entrapment in the casting area is minimal, with many regions showing no entrapment at all. Castings produced under this condition should exhibit the best performance and fewer defects.

mm	m/s	mm	m/s	mm	m/s	mm	m/s
0	0.00	0	0.00	0	0.00	0	0.00
10	0.20	30	0.20	50	0.20	60	0.20
370	0.30	370	0.30	370	0.30	370	0.30
405	3.60	405	3.60	405	3.60	405	3.60
450	3.60	450	3.60	450	3.60	450	3.60
460	0.15	460	0.15	460	0.15	460	0.15
470	0.10	470	0.10	470	0.10	470	0.10
480	0.00	480	0.00	480	0.00	480	0.00

No. 1		No. 2		No. 3		No. 4	
mm	m/s	mm	m/s	mm	m/s	mm	m/s
0	0.00	0	0.00				
50	0.30	50	0.04				
370	0.30	370	0.30				
405	3.60	405	3.60				
450	3.60	450	3.60				
460	0.15	460	0.15				
470	0.10	470	0.10				
480	0.00	480	0.00				

The first column is the piston position, and the second column is the piston movement speed

Figure 12. Six-piston slow-shot acceleration modes.

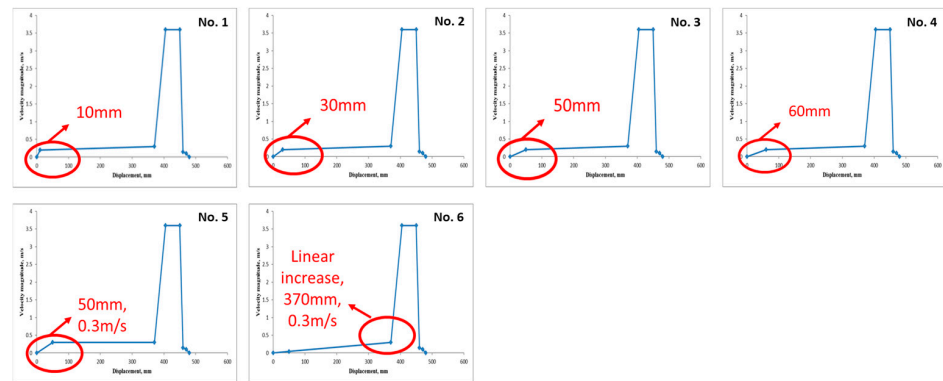


Figure 13. The relationship between displacement and velocity under 6 piston slow shot acceleration modes.

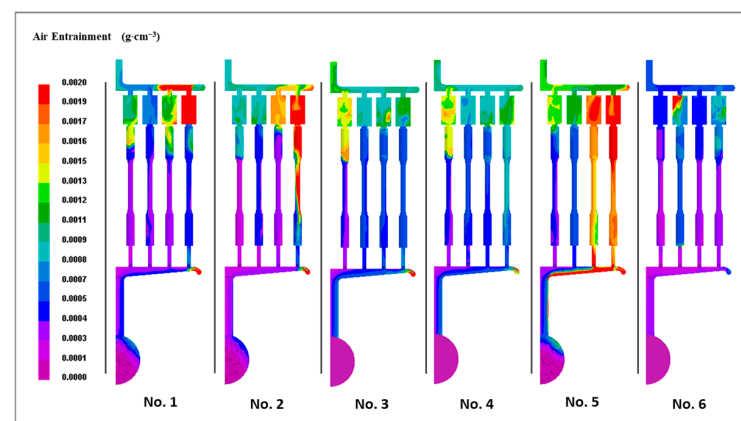


Figure 14. Air entrapment at the casting mold under 6 piston slow shot acceleration modes.

#### 4.5. Optimal Process Parameters to Reduce the Combustion of Lubricants on the Final Product Quality

To achieve better final sample quality, it is essential to select the most suitable process parameters, primarily including slow-shot velocity and slow-shot acceleration profiles. Based on the results of the completed numerical simulations, the following observations

were made. Low velocity (0.2–0.3 m/s): This condition results in less air entrainment but higher oxide inclusions, making it suitable for castings with high surface quality requirements. Medium velocity (0.4–0.6 m/s): Air entrainment and oxide inclusions are relatively balanced in this range, making it the most optimized velocity range for castings with comprehensive performance requirements. High velocity (0.6–1.0 m/s): Air entrainment significantly increases, and oxide inclusions also become more prevalent. This condition is suitable for producing castings where internal porosity and inclusions are less critical. For general cases, the optimal slow-shot velocity is found to be in the range of 0.4–0.6 m/s. Regarding the slow shot acceleration profile, the most favorable casting performance corresponds to condition 6, where the slow shot velocity accelerates from 0 to 0.3 m/s over 0–370 mm during the slow-shot phase. This optimized method can be applied to various high-pressure die casting processes, regardless of the specific casting size or design. To achieve the best process parameters, simulations can be conducted to assess the impact of lubricant combustion, oxide inclusions, and air entrainment, followed by adjustments to minimize negative effects.

## 5. Conclusions

This study presents a detailed analysis of the impact of piston lubricant combustion on defect formation in the cold chamber high-pressure die casting process. The results reveal that the combustion of piston lubricants leads to the generation of gas bubbles and non-metallic inclusions, which are transported into the die cavity and subsequently trapped in the castings. These defects significantly influence the mechanical properties of the final product, primarily through the formation of porosity and oxide inclusions.

1. The effects of lubricant combustion can be observed using material characterization techniques such as SEM and EDS. Furthermore, numerical simulations based on finite element modeling can be used to predict the distribution of these defects under various process parameters. The simulations also provided insight into the effect of different slow shot velocities and acceleration profiles on defect formation. Based on the findings, the optimal process parameters for minimizing the impact of lubricant combustion on product quality were identified. Specifically, a slow-shot velocity range of 0.4–0.6 m/s and an acceleration profile that ramps up to 0.3 m/s over 0–370 mm of the shot sleeve proved to be the most effective in reducing air entrainment and oxide inclusions.
2. This research provides valuable insights into the complex interactions between piston lubricants, melt flow, and defect formation in HPDC. The optimized process parameters identified in this study offer a practical solution for improving the quality of castings, particularly in industries where surface finish and mechanical integrity are of utmost importance. Future research should focus on developing advanced, low-combustion lubricants to reduce gas and oxide inclusions, while integrating real-time monitoring systems for dynamic defect control. Additionally, studying the effects of complex geometries, alloy compositions, and sustainable practices could enhance casting quality and reduce environmental impact. Scaling experimental findings to industrial applications will be essential for bridging the gap between laboratory research and real-world production.

**Author Contributions:** Conceptualization, K.D.; methodology, K.D.; software, K.D.; validation, K.D., E.L. and Z.F.; formal analysis, Z.F.; investigation, J.L.; resources, K.D.; data curation, Y.Z.; writing—original draft preparation, J.L.; writing—review and editing, K.D.; visualization, J.L.; supervision, K.D., E.L. and Z.F.; project administration, K.D.; funding acquisition, Z.F. All authors have read and agreed to the published version of the manuscript.

**Funding:** This research was funded by the National Science Foundation of China (52304360) and the Open foundation of the State Key Laboratory of Advanced Metallurgy, University of Science and Technology Beijing, China (K22-07), the Key Research and Development Program of Xiangjiang Laboratory (22XJ01002), and Engineering and Physical Sciences Research Council (EPSRC) and Jaguar Land Rover Ltd. [grant number 11055100].

**Informed Consent Statement:** Informed consent was obtained from all subjects involved in the study.

**Data Availability Statement:** The original contributions presented in the study are included in the article, further inquiries can be directed to the corresponding author.

**Acknowledgments:** The technical support from UK site of ESI Group is greatly appreciated for software usage and model application. And the experiment apparatus supplied by BCAST, Brunel University London is also acknowledged.

**Conflicts of Interest:** The authors declare no conflicts of interest.

## References

1. Anglada, E.; Meléndez, A.; Vicario, I.; Idoiaga, J.K.; Mugarza, A.; Arratibel, E. Prediction and Validation of Shape Distortions in the Simulation of High Pressure Die Casting. *J. Manuf. Process.* **2018**, *33*, 228–237. [[CrossRef](#)]
2. Jarfors, A.E.W.; Tong, S.; Hu, B.; Nagendra Sharma, S.; Wee, C. Mechanism of Lubrication-Induced Surface Cracking in Hot Chamber Die Cast Thin-Walled AZ91D Parts. *Mater. Manuf. Process.* **2003**, *18*, 637–641. [[CrossRef](#)]
3. Wang, L.; Turnley, P.; Savage, G. Gas Content in High Pressure Die Castings. *J. Mater. Process. Technol.* **2011**, *211*, 1510–1515. [[CrossRef](#)]
4. Lugscheider, E.; Barimani, C.; Guerreiro, S.; Bobzin, K. Corrosion Tests of PVD Coatings with Die Lubricant Used for Al High-Pressure Die-Casting Dies. *Surf. Coat. Technol.* **1998**, *108–109*, 408–412. [[CrossRef](#)]
5. Dybowski, B.; Kielbus, A.; Poloczek, Ł. Effects of Die-Casting Defects on the Blister Formation in High-Pressure Die-Casting Aluminum Structural Components. *Eng. Fail. Anal.* **2023**, *150*, 107223. [[CrossRef](#)]
6. Tian, C.; Law, J.; van der Touw, J.; Murray, M.; Yao, J.-Y.; Graham, D.; St. John, D. Effect of Melt Cleanliness on the Formation of Porosity Defects in Automotive Aluminium High Pressure Die Castings. *J. Mater. Process. Technol.* **2002**, *122*, 82–93. [[CrossRef](#)]
7. Wu, M.; Li, X.; Guo, Z.; Xiong, S. Effects of Process Parameters on Morphology and Distribution of Externally Solidified Crystals in Microstructure of Magnesium Alloy Die Castings. *China Foundry* **2018**, *15*, 139–144. [[CrossRef](#)]
8. Ahn, C.; Jo, I.; Ji, C.; Cho, S.; Mishra, B.; Lee, E. Creep Behavior of High-Pressure Die-Cast AlSi10MnMg Aluminum Alloy. *Mater. Charact.* **2020**, *167*, 110495. [[CrossRef](#)]
9. Gourlay, C.M.; Laukli, H.I.; Dahle, A.K. Defect Band Characteristics in Mg-Al and Al-Si High-Pressure Die Castings. *Metall. Mater. Trans. A* **2007**, *38*, 1833–1844. [[CrossRef](#)]
10. Tsoukalas, V. The Effect of Die Casting Machine Parameters on Porosity of Aluminium Die Castings. *Int. J. Cast Met. Res.* **2003**, *15*, 581–588. [[CrossRef](#)]
11. Jiao, X.Y.; Wang, J.; Liu, C.; Guo, Z.; Wang, J.; Wang, Z.; Gao, J.; Xiong, S.M. Influence of Slow-Shot Speed on PSPs and Porosity of AlSi17Cu2.5 Alloy during High Pressure Die Casting. *J. Mater. Process. Technol.* **2019**, *268*, 63–69. [[CrossRef](#)]
12. Fiorese, E.; Bonollo, F. Plunger Kinematic Parameters Affecting Quality of High-Pressure Die-Cast Aluminum Alloys. *Metall. Mater. Trans. A* **2016**, *47*, 3731–3743. [[CrossRef](#)]
13. Cleary, P.W.; Ha, J.; Prakash, M.; Nguyen, T. Short Shots and Industrial Case Studies: Understanding Fluid Flow and Solidification in High Pressure Die Casting. *Appl. Math. Model.* **2010**, *34*, 2018–2033. [[CrossRef](#)]
14. Pereira, G.G.; Cleary, P.W.; Serizawa, Y. Prediction of Fluid Flow through and Jet Formation from a High Pressure Nozzle Using Smoothed Particle Hydrodynamics. *Chem. Eng. Sci.* **2018**, *178*, 12–26. [[CrossRef](#)]
15. Cica, D.; Kramar, D. Intelligent Process Modeling and Optimization of Porosity Formation in High-Pressure Die Casting. *Int. J. Met.* **2018**, *12*, 814–824. [[CrossRef](#)]
16. Li, X.; Guo, Z.; Xiong, S. Influence of Melt Flow on the Formation of Defect Band in High Pressure Die Casting of AZ91D Magnesium Alloy. *Mater. Charact.* **2017**, *129*, 344–352. [[CrossRef](#)]
17. Xu, H.; Liu, W.; Wang, Y.; Ma, S.; Yuan, C.; Jia, H.; Cheng, X.; Wang, R. Control and Optimization of Defects in Die Casting of Complicated Right Crankcase Cover. *J. Mater. Res. Technol.* **2024**, *33*, 2831–2840. [[CrossRef](#)]
18. Niu, Z.; Liu, G.; Li, T.; Ji, S. Effect of High Pressure Die Casting on the Castability, Defects and Mechanical Properties of Aluminium Alloys in Extra-Large Thin-Wall Castings. *J. Mater. Process. Technol.* **2022**, *303*, 117525. [[CrossRef](#)]
19. Lordan, E.; Dou, K.; Zhang, Y.; Tzileroglou, C.; Jacot, A.; Blake, P.; Fan, Z. Turbulent Breakup of Non-Metallic Inclusions and Equiaxed Crystals during Solidification of a Hypoeutectic Al-Si Alloy. *Materialia* **2021**, *17*, 101114. [[CrossRef](#)]

20. Zhang, Y.; Lordan, E.; Dou, K.; Wang, S.; Fan, Z. Influence of Porosity Characteristics on the Variability in Mechanical Properties of High Pressure Die Casting (HPDC) AlSi7MgMn Alloys. *J. Manuf. Process.* **2020**, *56*, 500–509. [[CrossRef](#)]
21. ASTM International Home Page. Available online: <https://www.astm.org/> (accessed on 21 February 2025).
22. Pequet, C.; Rappaz, M.; Gremaud, M. Modeling of Microporosity, Macroporosity, and Pipe-Shrinkage Formation during the Solidification of Alloys Using a Mushy-Zone Refinement Method: Applications to Aluminum Alloys. *Metall. Mater. Trans. A* **2002**, *33*, 2095–2106. [[CrossRef](#)]
23. Homayonifar, P.; Babaei, R.; Attar, E.; Shahinfar, S.; Davami, P. Numerical Modeling of Splashing and Air Entrapment in High-Pressure Die Casting. *Int. J. Adv. Manuf. Technol.* **2008**, *39*, 219–228. [[CrossRef](#)]

**Disclaimer/Publisher’s Note:** The statements, opinions and data contained in all publications are solely those of the individual author(s) and contributor(s) and not of MDPI and/or the editor(s). MDPI and/or the editor(s) disclaim responsibility for any injury to people or property resulting from any ideas, methods, instructions or products referred to in the content.